INTERNATIONAL JOURNAL FOR NUMERICAL METHODS IN FLUIDS
Int. J. Numer. Meth. Fluids 2005; **48**:853–867
Published online 15 March 2005 in Wiley InterScience (www.interscience.wiley.com). DOI: 10.1002/fld.958

Numerical simulations of miscible fluids on a rotating Hele–Shaw cell with effects of Coriolis forces

Ching-Yao Chen[1,*,†] and Yu-Chia Liu[2]

[1]*Department of Mechanical Engineering, National Yunlin University of Science and Technology, Yunlin 640, Taiwan, R.O.C.*
[2]*Department of Mechanical and Automation Engineering, Da-Yeh University, Chang-Hua 515, Taiwan, R.O.C.*

SUMMARY

The effects of Coriolis forces to interfacial stabilities on miscible rotating Hele–Shaw flows are investigated by means of highly accurate numerical schemes. Two major influences on the interfaces, i.e. the stabilization of circumferential fingerings and the unstable body distortion of droplets, are observed. These two phenomena can be represented by two characteristic measurements, i.e. interfacial length and radius of gyration, respectively. Without an additional injection, the miscible interface is found to be more stable at higher Coriolis factors, based on both the judgments of growths in interfacial length and the radius of gyration. However, with an additional injection, a visible body distortion with suppressed interfacial fingerings at higher Coriolis factors leads to inconsistent developments in these two characteristic measurements. The stabilized effect of interfacial fingering delays and weakens the growth in interfacial length at higher Coriolis factors, while faster and greater growth in the radius of gyration is observed because of the significant body distortion. As a result, the effects of the Coriolis forces on the miscible interfacial instabilities should be addressed with great caution. Copyright © 2005 John Wiley & Sons, Ltd.

KEY WORDS: miscible fluids; rotating Hele–Shaw cell; fingering instabilities; Coriolis forces

1. INTRODUCTION

The Hele–Shaw flows driven by centrifugal force have been the subject of recent studies [1–4] due to their potential applications to the technology of spin-coating, i.e. precious metals for electronic wafers, or organic solvents for cleaning purposes. In the common practices of the spin-coating process, a liquid drop is initially deposited on the top of a rotating target substrate, and is spread outward by centrifugal force [5–8]. Since the coating film is ex-

*Correspondence to: Ching-Yao Chen, Department of Mechanical Engineering, National Yunlin University of Science and Technology, 123 University Road, Section 3, Touliu, Yunlin 640, Taiwan, R.O.C.
†E-mail: chingyao@yuntech.edu.tw

Contract/grant sponsor: ROC NSC; contract/grant number: 92-2212-E-224-012

Received 7 March 2004
Revised 14 October 2004
Accepted 31 January 2005

tremely thin, the approximation by lubrication theory yields to similar physical phenomenon to Hele–Shaw equations. Thus, the process of spin-coating bears great similarities to a rotating Hele–Shaw flow. Based on the Hele–Shaw theory, Schwartz [1] analysed an immiscible rotating Hele–Shaw flow by a simplified mathematical model including the effects of Coriolis forces and reported an independent fingering pattern in both the liquid viscosity and the cell spacing. Many breaking drops from the liquid mass have also been observed. Carrillo *et al.* [2] investigated the interfacial instabilities of immiscible fluids in a rotating cell both theoretically, in which Coriolis forces are neglected, and experimentally. Experiments in the radial displacement of a fluid annulus [3] have shown the strong dependence of instabilities on the wetting condition of the outer interface. In a dry cell, however, a scaling correlation can be formed between the capillary number and a dimensionless group that relates to centrifugal force and capillary force. The follow-up stability analysis [4] showed that the instabilities in two interfaces, in which the leading interface is density driven and the trailing is driven by viscosity, are coupled through the pressure field. The prediction of stability analysis was confirmed by the experimental results. An interesting emission of liquid droplets at the fingertip was observed as well. Simulations of similar flows in a fully miscible environment that is relevant to the cleaning of organic solvents are conducted in a reference frame rotating with the cell [9], in which Coriolis forces are not accounted for, and in an inertia reference frame by imposing an approximated rotating velocity [10] to analyse the control parameters systematically, such as rotating speed, mixing strength, viscosity contrast and injection rate. Without available experimental data for validation, some interesting comparisons between miscible and immiscible flows have been made on the basis of analogy between physical mechanisms of individual parameters and qualitative observations. Great qualitative similarities in the fingering patterns with the experimental results of immiscible situations of little surface tension has been found. Nevertheless, in contrast to the immiscible situations [1], the effects of finite viscosity contrast have been found to be significant in miscible simulations even though similar fingering distortions toward the rotating orientation and the breakup of tiny drops on the fingertip have also been found in miscible simulations on the inertia reference frame. Furthermore, simulations of both immiscible and miscible flows that account for the Coriolis forces [1, 10] have caught the experimental phenomena of emission of drops from fingertips, but distorted fingers with rotating orientation have not been shown in the immiscible experiments [2–4]. On the other hand, the zero-Coriolis simulations of miscible fluids [9] have led to fingering patterns with great similarities to the immiscible experiments but with no droplet emission. In addition, a major disagreement exists with regard to whether injection provides a stable mechanism. More stable interfaces have been obtained by immiscible theoretical analysis [3] and numerical simulations of miscible cases [9], both excluding the Coriolis forces, if a more viscous fluid is injected. However, immiscible experiments in real spin-coating with injection [7] have led to decreases in the critical radius at a high rotating Bond number, thereby suggesting more unstable situations. These discrepancies raise an important question concerning the role of the Coriolis forces in the process of rotating Hele–Shaw flows. In order to clarify and complete the influences of the Coriolis forces, a more mathematically correct model [1] and order of magnitudes of the Coriolis forces in practical processes are applied in the present study of miscible flows. The outline of this paper is as follows. After the formulation of the physical problem and review of the computational technique in Section 2, Section 3 focuses on the computational results and their interpretations. Conclusions are provided in Section 4.

2. PHYSICAL PROBLEM AND GOVERNING EQUATIONS

We study the interfacial dynamics of a heavier (density ρ_h) and more viscous (viscosity μ_h) droplet with initial diameter D_0, which is surrounded by a miscible fluid with less density and viscosity, denoted as ρ_l and μ_l, respectively, in a rotating Hele–Shaw cell as shown in Figure 1. A point source flow with volume strength Q per unit depth is injected through the centre of the cell. The effect of Taylor dispersion [11] is assumed significant across the narrow gap of the cell, thus averaging Hele–Shaw equations are applicable. The governing equations, in a reference frame rotating with the cell, of continuity, momentum of the augmented Hele–Shaw equations [1, 9] and concentration conservation take the forms

$$\nabla \cdot \mathbf{u} = 0 \tag{1}$$

$$\nabla p = -\frac{12}{b^2}\mu\mathbf{u} + \rho\hat{\omega}^2\mathbf{x} + 2\rho\hat{\boldsymbol{\omega}}\mathbf{e}_z \times \mathbf{u} \tag{2}$$

$$\frac{\partial c}{\partial t} + \nabla \cdot (\mathbf{u}c) = D\nabla^2 c \tag{3}$$

Here, $\mathbf{u}$ denotes the velocity vector, b the Hele–Shaw cell gap spacing, $\hat{\omega}$ the angular speed, $\mathbf{x}$ the position vector on x–y plane, $\mathbf{e}_z$ the unit vector in z-direction, c the concentration of lighter fluid, D the diffusion coefficient and p the pressure. The viscosity is indicated by μ. In addition to the conventional viscous term on the right-hand side of the Hele–Shaw equations (2), the extra second and third terms are the centrifugal forces and the Coriolis forces, respectively. Any unconventional stresses, such as those interfacial stresses postulated by Korteweg [12], are neglected. Even numerous studies that include the effects of Korteweg stresses have been conducted [13–22], results are not yet conclusive regarding expressions and magnitudes of the stresses. For now our goal is merely to evaluate the influences of Coriolis forces.

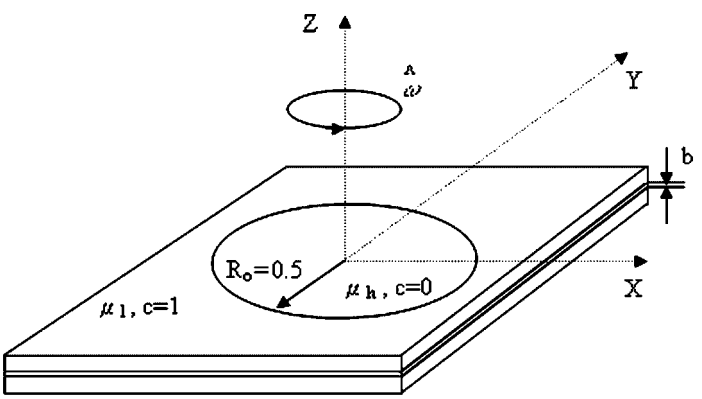

Figure 1. Principal sketch. A more viscous miscible droplet, with an original dimensionless radius of gyration $Ro = 0.5$ and surrounded by a less viscous fluid, is placed in a counter-clockwise rotating Hele–Shaw cell.

In order to render the governing equations dimensionless, we take the diameter D_0 of the droplet and the density difference $\Delta\rho = \rho_h - \rho_l$ as the characteristic scales. Two time scales are available at the present flow field, i.e. the rotating time scale $1/\hat{\omega}$, which is used by Chen and Wang [9, 10], and the scale $12\mu_l/b^2\Delta\rho\hat{\omega}^2$ of centrifugal-induced time [1]. Since the simulation is carried in the reference frame rotating with the cell, centrifugal-induced time is taken as a characteristic time scale in the present study. By further scaling with viscosity μ_l and pressure $\Delta\rho\hat{\omega}^2{D_0}^2$, a characteristic velocity scale $b^2\Delta\rho\hat{\omega}^2D_0/12\mu_l$ is obtained. For most mixtures, a linear density–concentration relationship represents a good approximation, and takes a form as

$$\rho(c) = c\rho_l + (1-c)\rho_h \tag{4}$$

For the dependence of viscosities on the concentration, an exponential relationship, which is commonly used by previous studies [23, 24], are assumed as

$$\mu(c) = \mu_l e^{R(1-c)}, \quad \mu_h = \mu_l e^R \tag{5}$$

The dimensionless momentum and concentration equations are rewritten in terms of vorticity (ω) and streamfunction (ψ), split into the potential component ψ_{pot} and rotational part ψ_{rot}, formulation

$$u = \frac{\partial\psi}{\partial y}, \quad v = -\frac{\partial\psi}{\partial x} \tag{6}$$

$$\psi = \psi_{pot} + \psi_{rot} \tag{7}$$

$$\nabla^2\psi_{rot} = -\omega \tag{8}$$

$$\omega = -R\nabla\psi\cdot\nabla c - \frac{1}{\mu}\left(y\frac{\partial c}{\partial x} - x\frac{\partial c}{\partial y}\right) - \frac{2Re}{\mu}\left(u\frac{\partial c}{\partial x} + v\frac{\partial c}{\partial y}\right) \tag{9}$$

$$\frac{\partial c}{\partial t} + \mathbf{u}\cdot\nabla c = \frac{1}{Pe}\nabla^2 c \tag{10}$$

$$\mu(c) = e^{R(1-c)}, \quad R = -\frac{1}{\mu}\frac{\mathrm{d}\mu}{\mathrm{d}c} \tag{11}$$

where u and v are the velocity components at x and y directions, respectively. The Peclet number Pe and Reynolds number Re take the forms

$$Pe = \frac{\Delta\rho\hat{\omega}^2b^2{D_0}^2}{12\mu_l D}, \quad Re = \frac{\Delta\rho\hat{\omega}b^2}{12\mu_l} \tag{12}$$

The analytical distribution of potential radial velocity v_{pot_r}, induced by a point source, is expressed as

$$v_{pot_r} = \frac{I}{r}, \quad I = \frac{6\mu_l Q}{\pi b^2\Delta\rho\hat{\omega}^2{D_0}^2} \tag{13}$$

where I is the dimensionless injecting strength. There are four dimensionless control parameters presented, such as the Peclet number Pe which can be interpreted as the dimensionless

rotating speed, the viscosity parameter R representing the viscosity contrast, and the Reynolds number Re which includes the effect of the Coriolis forces, and the effects of injecting volume by dimensionless injecting strength I. Here, focus is directed to the influences of the Coriolis factor Re and their coupled effects on other parameters.

The boundary conditions are prescribed as follows:

$$x = \pm 1 : \psi_{\text{rot}} = 0, \quad \frac{\partial c}{\partial x} = 0 \tag{14}$$

$$y = \pm 1 : \psi_{\text{rot}} = 0, \quad \frac{\partial c}{\partial y} = 0 \tag{15}$$

In order to reproduce the very fine structures of the fingers successfully, the highly accurate spectral method is applied. As a result, the actual boundary conditions applied in the numerical codes at $x = \pm 1$ are modified as $\partial\psi_{\text{rot}}/\partial x = 0$. Under the present situation where no concentration gradient is generated on these boundaries before the calculations terminated, the above conditions automatically lead to $\psi_{\text{rot}} = 0$. The initial conditions assume a circular droplet shape bounded by a steep concentration gradient in a form of error function. In order to break the unphysical artificial symmetry, a small magnitude of random noises is applied to the positions of 0.5 concentration. Results of testing simulations demonstrate that very insignificant influences of fingering patterns by the magnitude of noises. To solve the stream-function equation (8) by a pseudospectral method, a Galerkin-type discretization using cosine expansion is employed in the streamwise direction both on ω, and ψ. In the normal direction, discretization is accomplished by sixth-order compact finite differences. Vorticity equation (9) is evaluated by sixth-order compact finite difference schemes. A fully explicit third-order Runge–Kutta procedure on time and spatial sixth-order compact finite difference schemes are employed to solve the concentration equation (10). The set of equations are then solved and advanced in time. The numerical code is largely identical to the one used for earlier investigations [9, 10, 23–25], and is quantitatively validated by comparing the growth rates with the values obtained from the linear stability theory in a plane front [23–25]. In addition, the great qualitative similarities of the fingering features, reported in Chen and Wang [9, 10] as well as the results presented in the following section, to the relevant immiscible experiments also served as partial validation of the numerical schemes. More details on the implementation and quantitative validation of these schemes are provided by Chen and Meiburg [23], Ruith and Meiburg [24] and Meiburg and Chen [25].

3. RESULTS AND DISCUSSIONS

3.1. A rotating droplet

Representative calculations for $R = 2.5$ and $Pe = 10^4$ without additional injection $I = 0$ are firstly described. The R-value indicates that the droplet is about 12 times more viscous than the environmental fluid. In common spin-coating practices with a rotating frequency in the order of thousands rpm, the equivalent Reynolds numbers of the Coriolis forces are in the magnitude of $O(1)$, which are considered in the following simulations. The effects of the Coriolis forces

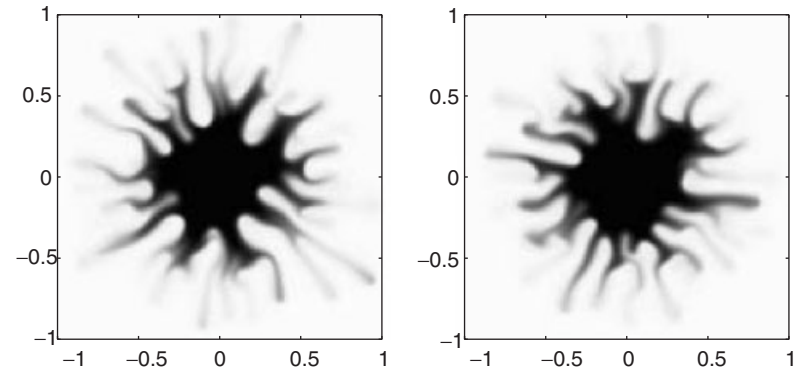

Figure 2. $Pe = 10^4$, $R = 2.5$ and $I = 0$. Concentration fields for: (a) $Re = 0$ at $t = 15.5$; and (b) $Re = 4$ at $t = 20$. Coriolis forces lead to slower-growing fingers that reach the computational boundaries at a much later time. Roots of fingers at $Re = 4$ appear thicker and more irregular.

are presented by different simulations of various Re, as shown in Figure 2. Similarly to the previous findings [9], very vigorous interfacial instability is triggered by the strong centrifugal force in the case of zero-Coriolis forces, shown in Figure 2(a), even the mixing front of the droplet is viscously stable. To conserve the mass, opposite fingers of the less viscous fluid penetrate toward the droplet origin. In the absence of the Coriolis forces, the radial fingers grow comparably in a straight outward trend and extend to the computational boundaries at about $t = 15.5$. The pattern of straight outward fingers without apparent distortion toward the rotational orientation is consistent with the experiments. Figure 2(b) displays the concentration field at strong Coriolis forces of $Re = 4$. The fingers move outward much slower compared to the previous non-Coriolis forces case, and they reach the computational boundaries at a much later time, $t = 20$. In addition, the roots of the fingers appear thicker and more irregular. The slimmer fingers as well as the faster outward movements at a lower Reynolds number indicate a stabilizing effect of the Coriolis forces. Similarly to immiscible situations, the effects of stabilization can also be confirmed by the growths in two characteristic quantities, such as the mixing interfacial length L and the radius of gyration Ro. However, unlike the immiscible case when a clear interface can be defined, the mixing region of miscible fluids is a layer. No accurate interfacial length and radius of gyration can be measured. Nevertheless, in the region of significant concentration gradient, the mixing length can be well represented as

$$L(t) = \iint \left(\left(\frac{\partial c}{\partial x} \right)^2 + \left(\frac{\partial c}{\partial y} \right)^2 \right)^{1/2} \mathrm{d}x\, \mathrm{d}y \tag{16}$$

as well as the radius of gyration Ro obtained by calculating half distance between the values of 0.99 averaging concentration across the y-direction, i.e. x_1, x_2 at $c_a = 0.99$ and

$$c_a(x) = \int c(x, y)\, \mathrm{d}y, \quad Ro = \frac{x_2 - x_1}{2} \tag{17}$$

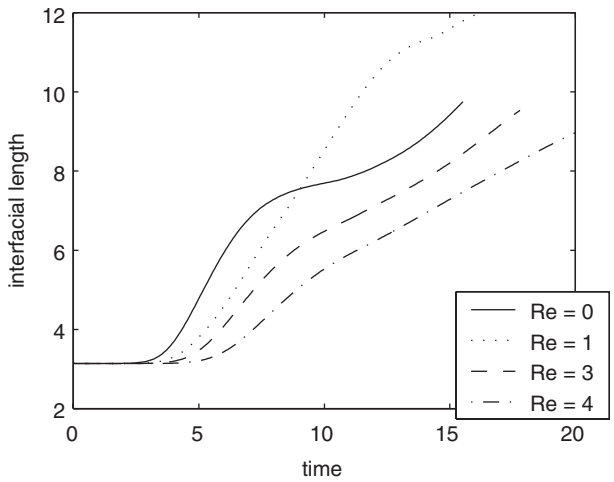

Figure 3. $Pe = 10^4$, $R = 2.5$ and $I = 0$. Temporal evolution of interfacial length. More rapid growth of $Re = 0$ reflects a more vigorous interfacial fingering.

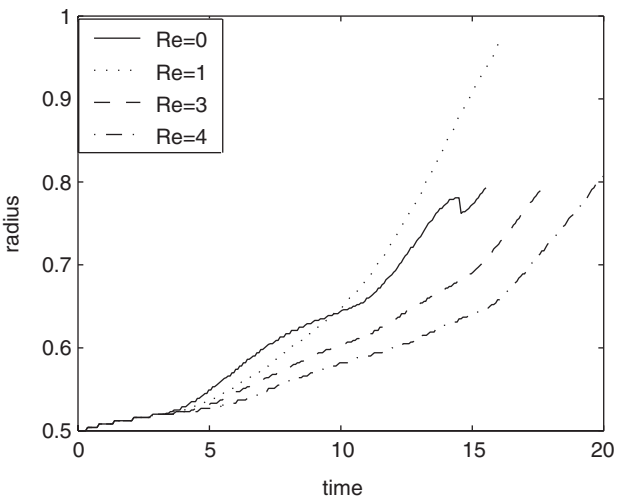

Figure 4. $Pe = 10^4$, $R = 2.5$ and $I = 0$. Temporal evolution of radius of gyration. Significant growth of radius is seen at a lower Reynolds number that represents stronger body distortion of droplet.

The growths of these two measurements are shown in Figures 3 and 4. The interfacial length starts to increase once the fingering instability is triggered, therefore an earlier growth and higher growth rate of interfacial length reflect a more unstable interface. In addition, the occurrence of instability also leads to a longer radius of gyration. As a result, the interfacial length is a good indication of the interfacial fingerings, the radius of gyration could well represent the body elongation of the droplet. Both these two characteristic quantities show

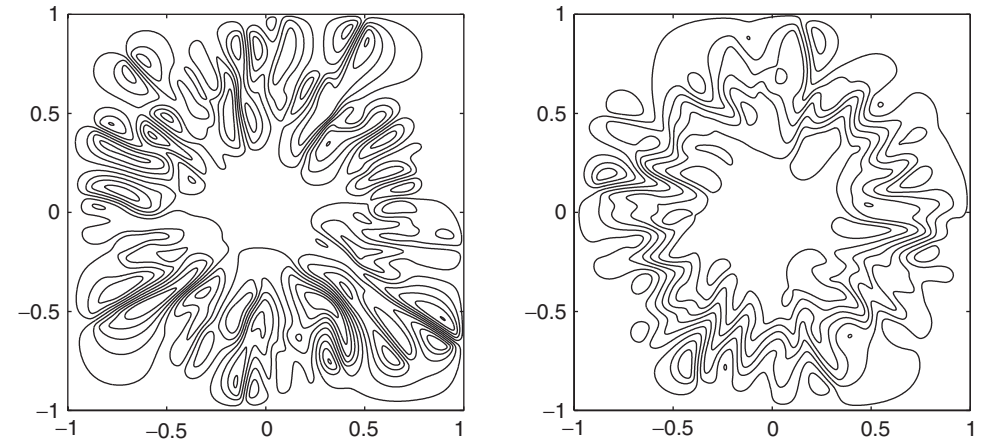

Figure 5. $Pe = 10^4$, $R = 2.5$ and $I = 0$. Contours of rotational streamfunction for: (a) $Re = 0$ at $t = 15.5$; and (b) $Re = 4$ at $t = 20$. Numerous independent eddy pairs which result to formation of fingers are observed with absence of Coriolis forces. On the other hand, presence of Coriolis forces lead to connected tangential streamlines and stabilized influences.

earlier and rapider growths that are attributed to less stable mixing interfaces at weaker Coriolis forces. However, one should note that even though the growths of these two measurements give a good judgment regarding the vigorousness of fingerings, they might be only suitable for the situations of high concentration gradients. As reasons stated above that miscible interfacial length and radius of gyration are merely approximations by calculating their concentration averages and gradients. This approximation might break down once the dispersion is strong such as the regions of thin fingers at later times. As shown in Figure 2(a), even the fingers are visually longer at $Re = 0$, the insignificant concentration magnitude caused by stronger mixing at the finger tip region leads to underestimated interfacial length and radius. It explains the line crosses of both interfacial length and radius of gyration for $Re = 0$ and 1 at later time period. The stabilized mechanism of Coriolis forces can be understood by the tangential shear effects to the mixing interfaces. Rogerson and Meiburg [26] have found that tangential shear stabilizes a plane mixing interface. In the present situation, the Coriolis forces are oriented perpendicularly to both the rotating axis (z-direction) and the local velocity (radial-direction), as expressed in Equation (2). A tangential shear results from the Coriolis forces, and stabilizes the mixing interface. Figure 5shows the streamlines of rotational components for the cases reported in Figure 2. Without the considerations of Coriolis forces ($Re = 0$) as shown in Figure 5(a), the rotational part of streamlines is on the formation of independent eddy pairs, which each pair leads to the growth of a finger. On the other hand, the presence of Coriolis forces provides a tangential shear force, and results in a connected circumferential streamline pattern. This tangential shear also delays the outward growth of fingers by pulling their sides, thereby leading to more irregular and thicker finger roots. However, emission of little drops on the fingertip is not found for the highest Re simulated here.

The influences of Coriolis factors at different rotating speeds and viscosity contrasts are also simulated. Since the local Coriolis forces are proportional to the radial velocity, which is

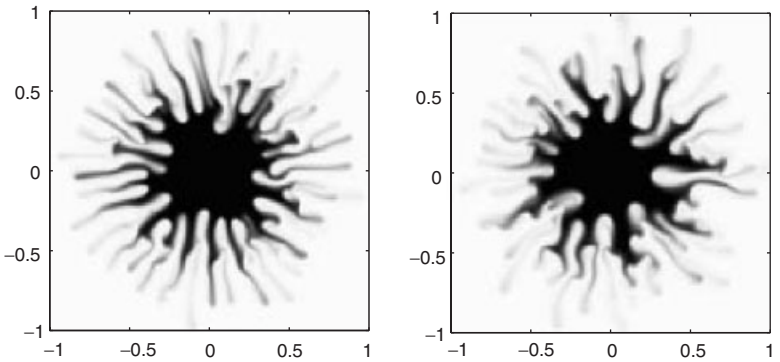

Figure 6. $Pe = 2.5 \times 10^4$, $R = 2.5$ and $I = 0$. Concentration fields for: (a) $Re = 0$ at $t = 12$; and (b) $Re = 4$ at $t = 16$. Stabilizing effects of Coriolis forces are confirmed at present higher rotating speed.

induced by the fingering instability, the effects of the Coriolis forces are expected more significantly at a higher Pe, which represents a stronger centrifugal force, and a lower viscosity parameter R, which provides a weaker viscous damping. Figures 6(a) and (b) show the fingering patterns for $Re = 0$ and 4, respectively, at the higher rotating speed of $Pe = 2.5 \times 10^4$. When comparing the concentration images to their counterparts with lower rotating speeds displayed in Figures 2(a) and (b), the fingering instabilities are seen to be more enhanced at the present higher Pe number, which confirms the previous study [9]. In addition, induced by a stronger rotating speed, the effects of the Coriolis forces are more pronounced in the current situation in which an apparent trend of tangential pulling forces leads to more irregular fingering developments, when compared to the straight outward growth at $Re = 0$. Similar influences of stabilization, indicated by a slower fingering movement, as well as thicker finger roots result from the presence of the Coriolis forces. The results for a lower viscosity contrast $R = 1$, while the rest of the control parameters, kept identical to the representative cases, are displayed in Figures 7(a) and (b). Similarly to the previous findings [9, 10], in which more vigorous fingerings are induced because of weaker viscous damping effects, the overall instabilities are stronger compared to the reference cases in Figure 2. Induced by stronger radial growths of fingers, the stabilizing effects of Coriolis forces are even more significant associated with identifiable counter-clockwise-orientated fingers. The two quantitative measurements, interfacial length and radius, also appear as slower developments at higher Coriolis forces for both situations of higher rotating speed and lower viscosity contrast, which confirms the stabilizing effects of the Coriolis forces.

3.2. Effects of injection

Focus is now directed to the flows with injection. The common spin coating process, which the layer of coating fluid keeps thinning and spreads outward, bears similarities to the injecting situations. In the absence of the Coriolis forces, injection of a more viscous fluid provides stronger viscous damping effects. Figures 8(a) and (b) show the fingering patterns at injecting strength $I = 0.01$ with the rest of the parameters kept identical to the representative cases in Figures 2(a) and (b). As mentioned previously, the magnitude of the local Coriolis forces is

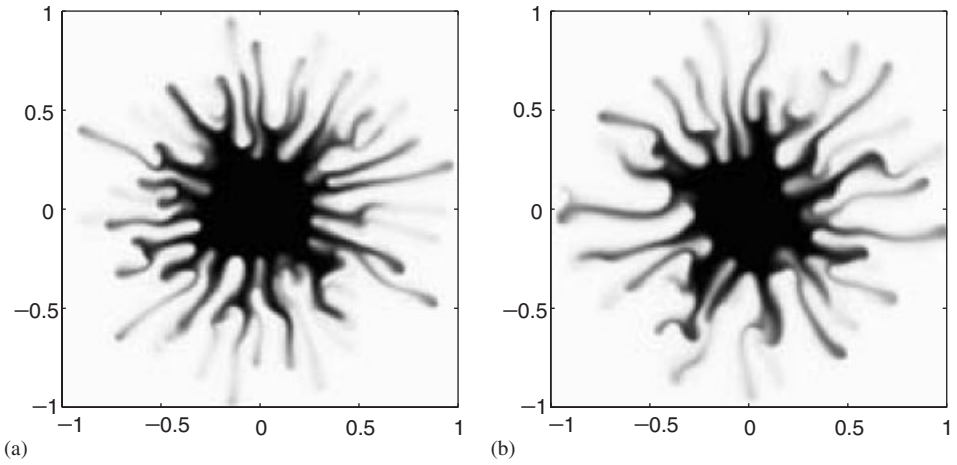

Figure 7. $Pe = 10^4$, $R = 1$ and $I = 0$. Concentration fields for: (a) $Re = 0$ at $t = 6.4$; and (b) $Re = 2$ at $t = 9.8$. Overall instabilities are stronger compared to reference cases in Figure 2, due to weaker viscous damping effects. Induced by stronger radial growths of fingers, stabilized effects of Coriolis forces are even more significant when associated with identifiable counter-clockwise-orientated fingers.

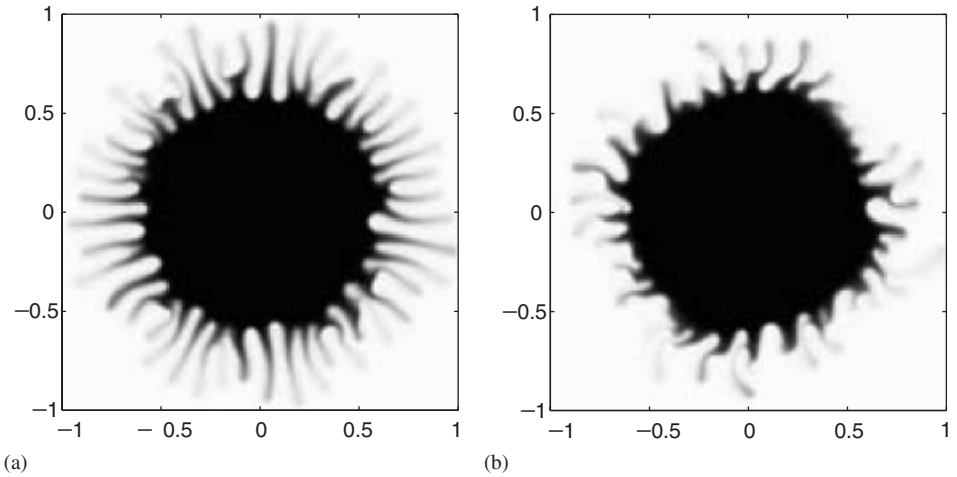

Figure 8. $Pe = 10^4$, $R = 2.5$ and $I = 0.01$. Concentration fields for: (a) $Re = 0$ at $t = 11$; and (b) $Re = 4$ at $t = 9.8$. Overall fingering instabilities appear visibly less vigorous at higher Coriolis parameter $Re = 4$ with distinguished fingering orientation of rotation. While nearly circular circumference of droplet body is preserved at $Re = 0$, displayed in Figure 7(a), stronger local Coriolis forces lead to clear body distortion of droplet at $Re = 4$. Similar fingering features are observed on the immiscible spin coating experiments [5] and simulations [8].

proportional to the local radial velocity and applies to the tangential direction; the additional injection provides a greater increase in radial velocity and, therefore, significant enhancement of the Coriolis forces. The overall fingering instabilities appear visibly less vigorous at the higher Coriolis parameter $Re = 4$ shown in Figure 8(b), compared to the $Re = 0$ of Figure 8(a)

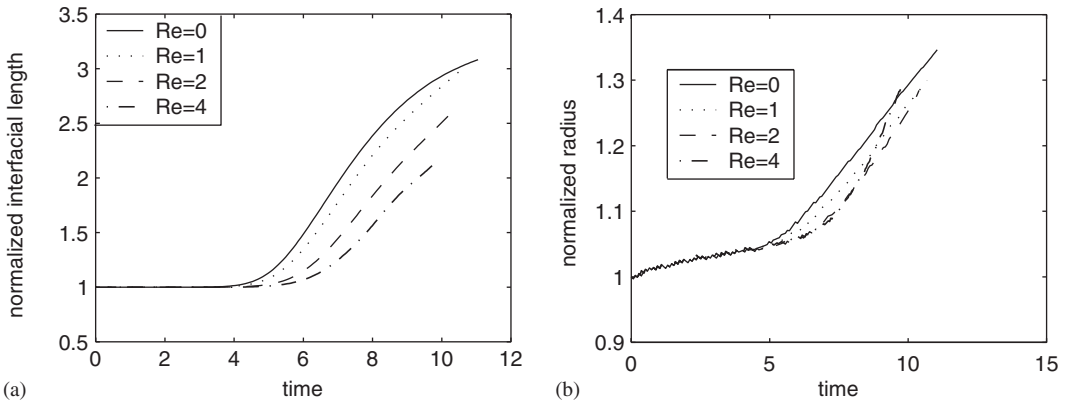

Figure 9. $Pe = 10^4$, $R = 2.5$ and $I = 0.01$ at various Coriolis factors. Temporal evolution of: (a) interfacial length; and (b) radius of gyration. Except for radius of $Re = 4$ at later stage, fact of later developments and slower growths for both measurements, which imply stabilized effects due to presence of Coriolis forces, is basically consistent with previous studies of zero-Coriolis forces. Inconsistency of rapid growth of radius for $Re = 4$ at later stage and earlier arrival to boundary are mainly caused by distortion of droplet body.

which is in line with the findings with no additional injection described earlier. It is interesting to notice that a distinguished fingering orientation of rotation results in fingering 8(b). While a nearly circular circumference of the droplet body is preserved in the zero-Coriolis forces case displayed in Figure 8(a), stronger local Coriolis forces lead to a clear body distortion of the droplet at $Re = 4$ shown in Figure 8(b). Similar shape of body distortion is also observed at the immiscible spin coating experiments [5] and simulations [8]. The distortion of the main body of the droplet at stronger Coriolis forces results in an earlier arrival of the heavier fluid to the computational domain, $t = 9.8$ for $Re = 4$, compared with $t = 11$ for $Re = 0$, which is inconsistent with the findings in non-injection situations. The quantitative measurements from normalized mixing interfacial length (L_n) and radius of gyration (Ro_n), normalized by the expanding rate caused by the injection strength I, such as

$$L_n(t) = \frac{L(t)}{2\pi\sqrt{2It + 1/4}}, \quad Ro_n(t) = \frac{Ro(t)}{\sqrt{2It + 1/4}} \tag{18}$$

are plotted in Figures 9(a) and (b). Except for the radius of $Re = 4$ at the later stage, the fact of later developments and slower growths for both measurements, which imply stabilized effects due to the presence of Coriolis forces, is basically consistent with the previous studies of zero-Coriolis forces. The inconsistency of the rapid growth of the radius for $Re = 4$ at the later stage and the earlier arrival to the boundary are mainly caused by the distortion of the droplet body. As mentioned previously, the representation of interfacial length is to determine circumferential instability, the growth of the radius of gyration represents the distortion of the droplet body. While the very strong tangential Coriolis forces prevent the vigorous growth of circumferential fingerings, thereby leading to less growth in interfacial length, as depicted in Figure 9(a), in the meantime the main body of the droplet is distorted by the significant Coriolis forces and results in a faster growth of the radius, as displayed in Figure 9(b). The

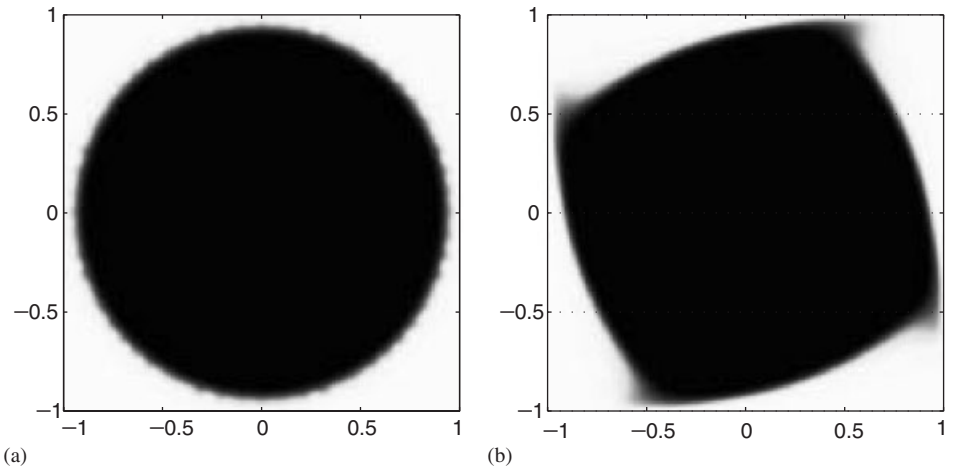

Figure 10. $Pe = 10^4$, $R = 2.5$ and $I = 0.05$. Concentration fields for: (a) $Re = 0$ at $t = 6.2$; and (b) $Re = 4$ at $t = 6.4$. Effect of body distortion is apparent even at present higher injecting rate. Enhanced viscous stabilization by stronger injection leads to no apparent fingering for both cases. However, compared to almost circular body shape at $Re = 0$, distortion toward rotating orientation is even more significant at $Re = 4$.

effect of body distortion is even apparent at a higher injecting rate, shown in Figure 10 with an injection of $I = 0.05$. The enhanced viscous stabilization by the stronger injection leads to no apparent fingering in both cases, as expected. However, compared to the almost circular body shape at zero-Coriolis forces in Figure 10(a), the distortion toward the rotating orientation is even more significant, as in Figure 10(b), due to the very significant Coriolis forces induced by stronger injection. These results suggest two main influences of the Coriolis forces. The Coriolis forces provide a stabilized tangential shear that suppresses the development of radial fingers on the circumference, which has also been confirmed by the previous no-injection cases. On the other hand, the sufficient strong Coriolis forces might also lead to a different kind of interfacial instability or distortion of the main body of the droplet. These two opposite effects can even be clearly identified by the simulations of smaller viscosity contrast $R = 1$, which would induce stronger local Coriolis forces, and $I = 0.05$, as shown in Figure 11(a) for $Re = 0$ and 11(b) for $Re = 2$. Very vigorous circumferential fingerings occur at zero-Coriolis forces, while significant droplet distortion with emission of drops on the fingertip, for which the pattern is quite similar to the immiscible simulations [1], results in the present case of very strong Coriolis forces. These two different effects lead to the opposite developments of interfacial length in Figure 12(a), and radius in Figure 12(b). Later and smaller growth of interfacial length is found at $Re = 0$, while the growth of the radius is observed to be earlier and higher at $Re = 2$. As a result, the effects of the Coriolis forces on a rotating interface are mixed and should be cautiously described.

These findings can be analogized to the available immiscible experiments and simulations, thereby resulting in a better explanation for the partial inconsistency mentioned in Section 1. Both the current studies and the immiscible simulations [1] lead to a rotating orientation fingering pattern with breaking droplets on the fingertips in cases of very stronger Coriolis

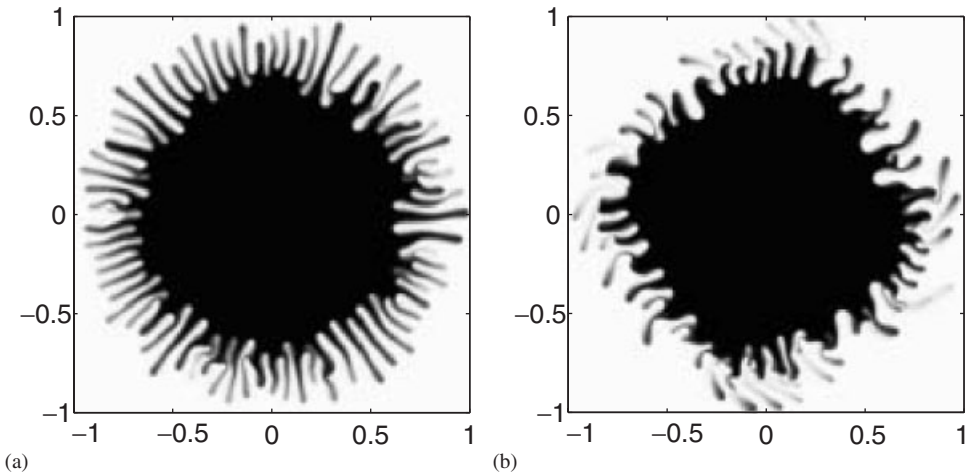

Figure 11. $Pe = 10^4$, $R = 1$ and $I = 0.05$. Concentration fields for: (a) $Re = 0$ at $t = 3.5$; and (b) $Re = 2$ at $t = 2.9$. Very vigorous circumferential fingerings occur at $Re = 0$, while significant droplet distortion with emission of drops on fingertips result in very strong Coriolis forces at $Re = 2$.

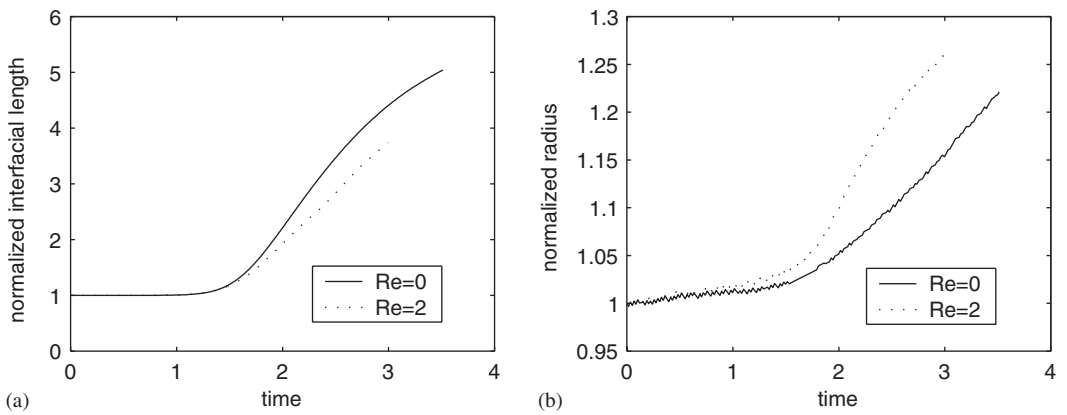

Figure 12. $Pe = 10^4$, $R = 1$ and $I = 0.05$ at various Coriolis factors. Temporal evolution of: (a) interfacial length; and (b) radius of gyration. Inconsistent evolutions of interfacial length and radius are observed. Later and smaller growth of interfacial length is found at $Re = 0$, while growth of radius is observed to be earlier and higher at $Re = 2$.

effects, such as the low viscosity contrast at high Coriolis factors. Even the emission of breaking droplets is also observed in the experiments [3], however, the phenomena of a rotating orientation fingering pattern is neither seen in immiscible Hele–Shaw experiments [2–4] nor spin coating experiments [7]. These discrepancies might be attributed to the insufficient magnitude of local Coriolis forces. As mentioned earlier, stronger Coriolis forces are not merely induced by the larger magnitudes of the Coriolis factor *Re* but also by the lower viscosity con-

trast that affects local radial velocity. While experiments [2–4] are conducted in relative low speed frequencies of $O(10^2)$, viscosity contrasts in the experiments of practical spin-coating processes [7] are very significant even the rotating speeds of $O(10^3)$, and thus generating weak local Coriolis forces. As a result, significant rotating fingering orientation does not occur in the experiments mentioned. Nevertheless, the sufficient Coriolis forces induced by the injection cause the droplet distortion and accelerate the growths of the radius of gyration. When considering the determination of stabilities in the spinning coating experiments [7] that are based mainly on the break in the circular shape, or the critical radius, the injection gives a more unstable judgment.

4. CONCLUSIONS

Numerical simulations of interfacial stabilities for miscible interfaces in a rotating Hele–Shaw cell by means of highly accurate numerical schemes have been presented. The centrifugal force, if the central fluid is heavier and in general more viscous, provides an unstable outward driving force, while the viscous effect tends to stabilize the contacting front. Since the orientation of the Coriolis forces apply tangentially to the droplet circumference, the effects of the Coriolis forces are found to have two major influences on the interfaces, the stabilization of circumferential fingerings and the body distortion of the droplet, which can be represented by two characteristic measurements, the interfacial length and the radius of gyration. In the Coriolis factors simulated, on the basis of practical magnitudes of the experiments, without additional injection the effect of stabilization of fingering instabilities is much more significant, compared to the body distortion on a rotating droplet. The miscible interface is found to be more stable, both on the conventional judgments of growth in interfacial length and radius of gyration at higher Coriolis factors. However, for stronger local Coriolis forces enhanced by additional injecting radial velocity, the body distortion is visible, while the interfacial fingerings are suppressed. With an additional injection, the occurrences of significant body distortion at higher Coriolis factors lead to inconsistent developments in the two characteristic measurements. The stabilized effect of interfacial fingering delays and weakens the growth of interfacial length at higher Coriolis factor. Faster and greater growth in the radius of gyration is observed because of the significant body distortion. As a result, the effects of the Coriolis forces on the miscible interfaces should be addressed with great caution.

ACKNOWLEDGEMENTS

The authors wish to express appreciation to Dr Cheryl Rutledge for her editorial assistance.

REFERENCES

1. Schwartz L. Instabilities and fingering in a rotating Hele–Shaw cell or porous medium. *Physics of Fluids A* 1989; **1**:167–169.
2. Carrillo L, Magdaleno F, Casademunt J, Ortin J. Experiments in a rotating Hele–Shaw cell. *Physical Review E* 1996; **54**:6260–6267.
3. Carrillo L, Soriano J, Ortin J. Radial displacement of a fluid annulus in a rotating Hele–Shaw cell. *Physics of Fluids* 1999; **11**(4):778–785.
4. Carrillo L, Soriano J, Ortin J. Interfacial instability of a fluid annulus in a rotating Hele–Shaw cell. *Physics of Fluids* 2000; **12**(7):1685–1698.

5. Fraysse N, Homsy G. An experimental study of rivulet instabilities in centrifugal spin coating of viscous Newtonian and non-Newtonian fluids. *Physics of Fluids A* 1994; **6**(4):1491–1504.
6. Spaid M, Homsy G. Stabilities of viscoelastic dynamic contact lines: an experimental study. *Physics of Fluids A* 1997; **9**(4):823–832.
7. Wang W, Chou F. Fingering instability and maximum radius at high rotational bond number. *Journal of the Electrochemical Society* 2001; **148**(5):G283–G290.
8. Schwartz L, Roy R. Theoretical and numerical results for spin coating of viscous liquids. *Physics of Fluids* 2004; **16**(3):569–584.
9. Chen C-Y, Wang S. Interfacial instabilities of miscible fluids in a rotating Hele–Shaw cell. *Fluid Dynamics Research* 2002; **30**(5):315–330.
10. Chen C-Y, Wang S. Stabilities of miscible interfaces in a rotating Hele–Shaw cell. *Transactions of the Aeronautical and Astronautical Society of ROC* 2002; **34**(3):239–245.
11. Taylor G. Dispersion of soluble matter in a solvent flowing slowly through tube. *Proceedings of the Royal Society of London Series A* 1953; **219**:186–203.
12. Korteweg D. Sur la forme que prennent les équations du mouvement des fluides si l'on tient compte des forces capillaires causées par des variations de densité. *Arch. Neerl. Sciences Exactes et Naturelles* 1901; **6**(II):1–24.
13. Davis H. A theory of tension at a miscible displacement front. Numerical simulation in oil recovery. *IMA Volumes in Mathematics and its Applications*, vol. 11. Springer: Berlin, 1988.
14. Galdi G, Joseph D, Prezisi L, Rionero S. Mathematical problems for miscible, incompressible fluids with Korteweg stresses. *European Journal of Mechanics B-Fluids* 1991; **10**:253–267.
15. Hu H, Joseph D. Miscible displacement in a Hele–Shaw cell. *Zeitschrift fur Angewandte Mathematik und Physik* 1992; **43**:626–645.
16. Joseph D, Renardy Y. *Fundamentals of Two-fluid Dynamics*, *Part II*. Springer: Berlin, 1992.
17. Joseph D, Hung A, Hu H. Non-solenoidal velocity effects and Korteweg stresses in simple mixture of incompressible liquids. *Physica D* 1996; **97**:104–125.
18. Petitjeans P. Une tension de surface pour les fluides miscibles. *Comptes Rendus de l'Academie des Sciences Paris Serie Iib* 1996; **322**:673–679.
19. Petitjeans P, Kurowski P. Fluides non miscibles/fluides miscibles: des similitudes interessantes. *Comptes Rendus de l'Academie des Sciences Paris Serie Iib* 1997; **325**:587–592.
20. Chen C-Y, Wang L, Meiburg E. Miscible droplets in a porous medium and the effect of Korteweg stresses. *Physics of Fluids* 2001; **13**(9):2447–2456.
21. Chen C-Y, Meiburg E. Miscible displacements in capillary tubes: influences of Korteweg stresses and divergence effects. *Physics of Fluids* 2002; **14**(7):2052–2058.
22. Chen C-Y. Numerical simulations of fingering instabilities in miscible magnetic fluids in a Hele–Shaw cell and the effects of Korteweg stresses. *Physics of Fluids* 2003; **15**(4):1086–1089.
23. Chen C-Y, Meiburg E. Miscible porous media displacements in the quarter five-spot configuration. Part 1: the homogeneous case. *Journal of Fluid Mechanics* 1998; **371**:233–268.
24. Ruith M, Meiburg E. Miscible rectilinear displacements with gravity override. Part 1: homogeneous porous medium. *Journal of Fluid Mechanics* 2000; **420**:225–257.
25. Meiburg E, Chen C-Y. High-accuracy implicit finite difference simulations of homogeneous and heterogeneous miscible porous media flows. *SPE Journal* 2000; **2**:129–137.
26. Rogerson A, Meiburg E. Shear stabilization of miscible displacement of processes in porous media. *Physics of Fluids A* 1993; **5**:1344–1355.

